Merging-limited coarsening governs long-term stability of nanoscale condensates

Feipeng Chen[1], Yaojun Zhang[2,3*], Ho Cheung Shum[1,4*]

[1]Department of Mechanical Engineering, The University of Hong Kong, Pokfulam Road, Hong Kong (SAR), China

[2]Department of Physics and Astronomy, Johns Hopkins University, Baltimore, MD 21218, USA

[3]Department of Biophysics, Johns Hopkins University, Baltimore, MD 21218, USA

[4]Advanced Biomedical Instrumentation Centre, Hong Kong Science Park, Shatin, New Territories, Hong Kong (SAR), China

*Corresponding author. Email: yaojunz@jhu.edu and ashum@hku.hk.

Abstract

Droplet coarsening occurs in a variety of fields, characterized by the spontaneous growth of smaller droplets into larger ones to minimize their interfacial free energy and achieve global thermodynamic equilibrium. However, recent studies revealed that the coarsening is much suppressed in living cells where nanoscale biomolecular condensates with droplet-like behaviors maintain stable sizes over extended time periods. The mechanism underpinning such long-term stability of condensates remains poorly understood. Here, we experimentally observe that coacervate droplets of small sizes (tens to hundreds of nanometers) remain stable over hours with significantly slower coarsening rates than predicted by classic theories. Using scaling analysis and Monte Carlo simulations, we demonstrate that the anomalously stable coacervates can be explained by a merging-limited coarsening (MLC), in which merging probability among coacervates of sizes smaller than a critical value $r_c \sim \sqrt{\eta/\gamma}$ becomes markedly low, where η is the

internal viscosity and γ is the interfacial tension of droplets. We further develop an analytical model that quantitatively captures the coarsening dynamics of coacervates across different experimental conditions. More broadly, by constructing a viscosity-interfacial tension diagram, we find that many biological condensates intrinsically exhibit large critical sizes, making them prone to undergo slow coarsening through the MLC mechanism. Such merging-limited coarsening may represent a universal mechanism underlying condensate size control in synthetic systems and living cells.

Introduction

Droplet coarsening occurs universally in many natural and industrial processes, from oil droplets swimming and coalescing in a stirred salad dressing, to water droplets condensing and merging on windows or steam engines. Coarsening is a spontaneous process wherein droplets merge and ripen over time driven by the system's tendency to minimize interfacial free energy and reach thermodynamic equilibrium. In a conventional picture, coarsening happens mainly through two mechanisms: Brownian motion-induced coalescence (BMC) of droplets [1-3] and Ostwald ripening driven by pressure gradients [4, 5]. There has been a growing emphasis on understanding analogous coarsening phenomena in living cells, prompted by the recent discovery of biomolecular condensates and their critical roles in cellular physiology and diseases [1, 4, 6-8]; in particular, many condensates exhibit liquid-like behaviors including fusing upon contact, wetting surfaces, and dripping under shear stresses [9-11].

In contrast to the conventional coarsening picture, many condensates in living cells maintain stable sizes and rarely coarsen over long time periods [1, 4, 12-14]. Given the complexity of the intracellular environment, many factors could influence condensate coarsening. For example, it has been proposed that sustained chemical reactions can actively stabilize droplet size [15-18], whereas the presence of chromatin in nucleus and actin filaments in cytoplasm can passively suppress both Brownian motion-induced merging and Ostwald ripening of condensates [1, 4, 13]. In another work, absorption of protein-RNA clusters onto condensate surfaces has been shown to generate "Pickering emulsions", wherein the absorbed clusters act like surfactants to reduce the surface tension and form patched physical barriers, collectively impeding the coarsening process [12, 19]. These aforementioned mechanisms rely on specific intracellular environments to suppress the coarsening. This then implies that condensates formed *in vitro* in the absence of these specific

conditions should coarsen fast following the conventional coarsening picture, which is indeed true for a majority of previously *in vitro* studies focusing on condensates of micrometers in size or larger [2].

Surprisingly, recent experiments revealed that nanoscale condensates comprised of various protein species can remain stable in pure aqueous solutions without coarsening [14, 20-24]. In these cases, the above mentioned mechanisms do not apply, yet the conventional coarsening theories, namely BMC and Ostwald ripening, also fail to explain the suppressed coarsening dynamics [25, 26]. As a result, the underlying mechanism that gives rise to the long-term stability of these tiny condensates becomes a puzzle. It is important to note that nanoscale condensates in cells have functional implications in a variety of biological contexts [7, 27], including postsynaptic density in neurotransmission [28], transcriptional condensates in gene transcription [26, 29, 30], and heterochromatin in chromatin compaction [31, 32]. Investigating the temporal evolution of nanoscale condensates is therefore particularly critical for unraveling the intriguingly slow coarsening behaviors, despite technical challenges that nanoscale condensates are typically beyond the detection limit of conventional experimental techniques, such as fluorescence microscope and UV-vis spectroscopy [7, 20].

In this work, we combine experiments, simulations, and analytical theory to reveal a general merging-limited coarsening (MLC) mechanism that governs the time evolution of nanoscale coacervates and enables their long-term stability. We first demonstrate that the observed suppressed growth of nanoscale coacervates is caused by the reduced merging between coacervate droplets of sizes below a threshold value $r_c \sim \sqrt{\eta/\gamma}$, determined by the dense-phase viscosity η and the interfacial tension γ of the system. We then derive a unified analytical equation that accounts for this size-dependent merging probability and quantitatively captures the time evolution of coacervates under different experimental conditions. Application of our findings to biological condensates suggests that many biomolecular condensates are located in the high critical size region in a generic viscosity-interfacial tension diagram, making them prone to undergo slow coarsening via the MLC mechanism. Our results highlight the underappreciated role of merging-limited coarsening in the condensate size control in both living and synthetic systems.

Results

Formation of nanoscale complex coacervates at low polyelectrolyte concentrations.

Many biological condensates are formed by the complex coacervation between proteins and nucleic acids via multivalent interactions [11, 33]. To understand the underlying physics of biological phase separation, complex coacervates comprised of oppositely charged polyelectrolytes have been widely employed as model systems due to their simplified physicochemical characteristics [34-36]. In particular, complex coacervates have been shown to display various representative features of biological condensates, such as efficient encapsulations of molecules [37], multiphase organizations [38], enhancement of biochemical reactions [39], aging kinetics [40], and cross-membrane transport [41].

In this work, we start with one type of complex coacervates comprised of negatively charged poly(methacrylic acid, sodium salt) (PMA) and positively charged poly(diallyldimethylammonium chloride) (PDDA) (Fig. 1b). The polyelectrolyte solutions are prepared separately and gently mixed at 1:1 stoichiometry ratio of monomer concentrations to form complex coacervates. The mean hydrodynamic diameters of PMA/PDDA coacervates formed immediately after mixing (d_{h0}) are measured using the dynamic light scattering (DLS) technique. DLS offers a non-invasive way to precisely measure the size of coacervates by analyzing the fluctuations in scattered light intensity caused by the Brownian motion of coacervates in solutions. Experimental results show that d_{h0} increases monotonically with the increasing monomer concentration (c_{m}) (Fig. 1c). To confirm the DLS results, we first visualize complex coacervates under an optical microscope at various concentrations. At a high concentration, $c_{\mathrm{m}} = 20$ mM, bright-field images clearly reveal micrometer-sized coacervates in the solution (Supplementary Fig. 1d). At intermediate concentrations, $c_{\mathrm{m}} = 0.5$ mM and 2 mM, the existence of nanoscale coacervates could be indicated by blurry shadow in the bright-field images (Supplementary Fig. 1b). However, nanoscale coacervates (i.e., below a few hundred nanometers) formed at lower concentrations are hardly observed by the optical microscope (Supplementary Fig. 1a). Transmission electron microscopy (TEM) is further applied to provide clear visual evidence of the formation of nanoscale coacervates in solutions. Coacervates diameters characterized from TEM images are comparable to d_{h0} measured by DLS (Fig. 1c and Supplementary Fig. 2). In magnified images, polymer brushes at the periphery and a condensed core are evidently identified, indicating a gradual density transition between coacervates and surrounding solutions (Supplementary Fig. 2d).

The coarsening dynamics of nanoscale coacervates is suppressed.

The observation of nanoscale coacervates at low polyelectrolyte concentrations is consistent with recent studies which have shown the formation of nanoscale clusters at low concentrations [23, 25, 42, 43]. However, how these nanoscale droplets evolve over time has not been clearly explored due to technical challenges. Here, we use DLS to monitor the time evolution of hydrodynamic diameters d_h of complex coacervates formed at various concentrations over a long-time duration, typically exceeding 12 hours. We note that phase separation generally initiates with a nucleation or spinodal decomposition stage, followed by a coarsening process at later stages [2, 3]. Given that the initial process is typically fast [20, 44, 45], experimental results recorded in this study primarily correspond to the later coarsening stage. The DLS measurements reveal that the d_h of microscale coacervates formed at $c_\mathrm{m} = 16$ mM increases with time as a power law with the exponent close to $1/3$ (Fig. 1d). Such coarsening behavior has been observed in previous studies and is well explained by classic theories, such as Brownian motion-induced coalescence (BMC) or Ostwald ripening [2, 3]. Surprisingly, at intermediate concentrations ($c_\mathrm{m} = 2$ mM and 5 mM), nanoscale coacervates (~200 nm) initially remain stable but grow abruptly in later stages. The power-law exponent for coarsening in later stages is apparently larger than $1/3$, contradicting predictions from BMC and Ostwald ripening theory (Fig. 1e). Even more strikingly, nanoscale coacervates formed at $c_\mathrm{m} = 0.1$ mM and $c_\mathrm{m} = 0.3$ mM are remarkably stable over a period of 12 hours with their hydrodynamic diameters d_h remaining at ~80 nm and ~150 nm, respectively (Fig. 1f).

To show the generality of these anomalous coarsening behaviors, we repeat experiments using another type of complex coacervate, which consists of poly(vinylsulfonicacid, sodium salt) (PVS) and poly(diallyldimethylammonium chloride) (PDDA) mixed at the neutral charge ratio. Experimental characterizations again show the formation of complex coacervates with d_h0 ranging from tens of nanometers to a few microns (Supplementary Fig. 3, Supplementary Fig. 4, and Supplementary Fig. 5). The aforementioned three different types of coarsening behaviors are again observed for PVS/PDDA coacervates with different initial hydrodynamic diameters using DLS (Supplementary Fig. 6). In addition to synthetic coacervates, these suppressed coarsening have also recently been identified in various protein condensates, exhibiting power-law exponents smaller than $1/3$ [14, 20-24]. In particular, some studies also echo that the stable nanoscale condensates are more likely to be formed at low macromolecular concentrations [21, 23]. These

results therefore suggest a general mechanism that gives rise to the observed slow coarsening phenomena.

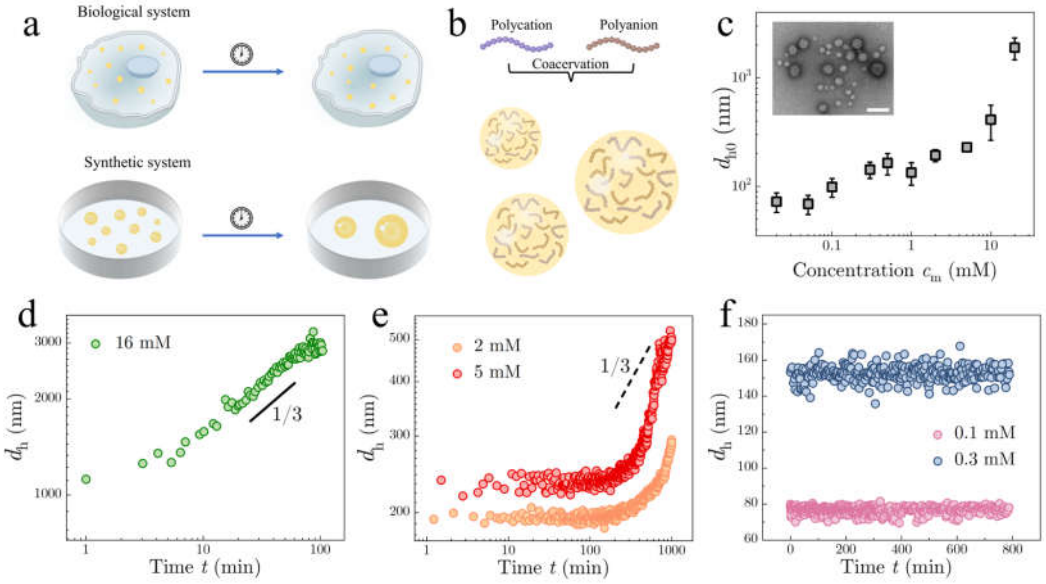

Fig. 1. Nanoscale complex coacervates formed at low concentrations exhibit suppressed coarsening. (a) Schematic diagram shows different coarsening dynamics of condensates in biological and synthetic systems, wherein the former remains stable over time while the latter merge and grow to larger ones. (b) Schematic of complex coacervates formed by mixing oppositely charged polycations and polyanions at a charge-balanced stoichiometry ratio. (c) The initial mean hydrodynamic diameter d_{h0} measured immediately after mixing as a function of monomer concentration of polyelectrolyte c_{m}. Error bars indicate mean ± standard deviation (SD) across at least three independent samples. Inset: TEM image shows sizes and spherical morphologies of nanoscale coacervates formed at $c_{\mathrm{m}} = 0.05$ mM. The white scale bar is 100 nm. (d) Coacervates formed at $c_{\mathrm{m}} = 16$ mM exhibit a power-law increase of the hydrodynamic diameter with time $d_{\mathrm{h}} \sim t^{\alpha}$ with the exponent $\alpha \approx 1/3$. (e) Coacervates formed at $c_{\mathrm{m}} = 2$ mM and $c_{\mathrm{m}} = 5$ mM are initially stable but increase abruptly in their hydrodynamic diameters in later times with power-law exponents seemingly larger than $1/3$. (f) Complex coacervates formed at $c_{\mathrm{m}} = 0.1$ mM and $c_{\mathrm{m}} = 0.3$ mM do not coarsen over time, i.e., their mean hydrodynamic diameters remain constant.

Merging-limited coarsening governs the time evolution of nanoscale coacervates.

To understand the mechanism that underlies these unexpected results, we start by reviewing two basic coarsening mechanisms: Brownian motion-induced coalescence (BMC) and Ostwald ripening. BMC is caused by coalescence of droplets that undergo stochastic Brownian motion [1-3], while Ostwald ripening is driven by flux of materials from smaller droplets to larger droplets due to the difference in their internal pressures and chemical potentials [1, 4, 5]. Theoretically, both mechanisms lead to a power-law scaling $r \sim kt^{1/3}$, where r is the mean radius of droplets, t

is the duration time, and k is a rate coefficient. However, the rate coefficients of different coarsening mechanisms, BMC (k_{BMC}) and Ostwald ripening (k_{OR}), depend on different physical parameters (Supplementary Note 1). Given physical parameters of complex coacervates in this work, we find that $k_{\mathrm{BMC}} \gtrsim 3.9 \times 10^{-6}\ \mu\mathrm{m}^3/\mathrm{s}$ and $k_{\mathrm{OR}} \approx 1.1 \times 10^{-7}\ \mu\mathrm{m}^3/\mathrm{s}$ (Supplementary Note 1). These estimates suggest that BMC contributes to the coarsening of coacervates more than Ostwald ripening, consistent with conclusions from previous studies that the effect of Ostwald ripening is generally negligible [1, 16]. We therefore neglect the effect of Ostwald ripening in the following sections and mainly focused on BMC as the coarsening mechanism.

The coarsening dynamics of microscale coacervates formed at $c_{\mathrm{m}} = 16$ mM (Fig. 1d) can be explained by the BMC mechanism, not only its power-law exponent is close to 1/3 but also the rate coefficient k is consistent with the theoretical estimate k_{BMC} (Supplementary Note 1). However, the coarsening of nanoscale coacervates formed at lower polyelectrolyte concentrations (Fig. 1e and 1f) is much slower than predicted by the BMC mechanism (Supplementary Fig. 7). Why is the coarsening of nanoscale coacervates suppressed? To answer that, we perform a scaling analysis to understand the physics behind the coalescence of droplets driven by Brownian motion. Droplets undergo Brownian motion in a solution due to the stochastic forces exerted by solvent molecules. When two droplets are in close proximity, they can either (i) merge with one another to form a larger droplet or (ii) diffuse away from each other (Fig. 2a). For case (i), the merging time τ_{m} between two droplets of the same radius r is estimated as $\tau_{\mathrm{m}} \sim r\eta/\gamma$ where η is the internal viscosity and γ is the interfacial tension of the droplets [12, 46]. Here we use this merging time as a proxy for the time needed for the two droplets to establish stable connection for merging. For case (ii), it takes a diffusion time $\tau_{\mathrm{d}} \sim r^2/D$ for the droplets to move away from each other by a distance r comparable to their size, over which the return probability of a droplet to its counterpart becomes low [47], where D is the diffusion coefficient of the droplets. Using the Stokes-Einstein equation $D = k_{\mathrm{B}}T/(6\pi\eta_0 r)$, we have $\tau_{\mathrm{d}} \sim 6\pi\eta_0 r^3/(k_{\mathrm{B}}T)$ where η_0 is the viscosity of the surrounding media.

In the above scaling analysis, the merging time τ_{m} increases linearly with the radius of droplet r whereas the diffusion time τ_{d} increases as r^3. Therefore, a critical size r_{c} emerges when $\tau_{\mathrm{m}} = \tau_{\mathrm{d}}$:

$$r_{\mathrm{c}} = \sqrt{\frac{\eta}{\gamma} \cdot \frac{k_{\mathrm{B}}T}{6\pi\eta_0}}. \tag{1}$$

The critical size r_c provides a quantitative threshold for distinguishing different coarsening mechanisms. When the mean droplet size $r > r_c$, the merging time is shorter than the diffusion time $\tau_m < \tau_d$, droplets are more likely to merge when encounter (Fig. 2b). Therefore, the coarsening process is mainly limited by the diffusion process that leads to droplet encounters, which is the assumption held by the theory of BMC. By contrast, when $r < r_c$, the merging time becomes longer than the diffusion time $\tau_m > \tau_d$, droplets are likely to diffuse away from nearby counterparts before merging happens (Fig. 2b). Consequently, the coarsening process is mostly limited by the probability of merging, which we term as the merging-limited coarsening (MLC) mechanism. What are the critical sizes of the coacervate systems in this work? To estimate r_c, we first measure the inverse capillary velocity η/γ with droplet fusion experiments (Supplementary Fig. 8), from which we then obtain $r_c \approx 334$ nm and 568 nm for the PMA/PDDA and PVS/PDDA systems, respectively. We therefore expect MLC to be relevant to nanoscale coacervates formed at low polyelectrolyte concentrations.

Can the MLC mechanism explain the observed suppressed coarsening of coacervates formed at low concentrations? To address this question, we perform Monte Carlo simulations to simulate the coarsening process of coacervate droplets. In our simulations, droplets diffuse randomly in a cubic box with periodic boundary conditions. The average amplitude of the displacement d over a time step Δt for individual droplets is set by the mean squared displacement (MSD), i.e., $d = \sqrt{6D\Delta t}$ with $D = k_B T/(6\pi\eta_0 r)$. To account for the dependence of merging efficiency E on droplet size r, we introduce a phenomenological relationship:

$$E(r) = e^{-\tau_m/\tau_d} = e^{-(r_c/r)^2}. \quad (2)$$

For large droplets when $r > r_c$ or $\tau_d > \tau_m$, E is close to unity so every collision results in a merging event. By contrast, for small droplets when $r < r_c$ or $\tau_d < \tau_m$, E becomes very small, and it then takes many collisions to lead to one successful merging event (Fig. 2b).

We start with a simulation where the initial mean radius of droplets $r_0 = r_c$. We find that droplets in our model merge and grow quickly (Fig. 2c), similar to results from the BMC mechanism. By contrast, when we take r_0 to be smaller than r_c ($r_0/r_c = 0.4$) to mimic the experimental cases of nanoscale coacervates, droplets in our model grow much slower than results from the BMC mechanism (Fig. 2d). We further plot the mean radius of droplets as a function of time for simulations at various initial conditions (Fig. 2e). The conventional BMC mechanism has $E = 1$, i.e., droplets merge readily upon contact. The mean radius of droplets increases as $r \sim t^{1/3}$

regardless of the initial droplet size r_0 (Fig. 2e, dashed lines). The MLC mechanism we proposed has a merging efficiency E that depends explicitly on the droplet size r in Eq. (2). When $r_0/r_c > 1$, the mean droplet size increases as a power law $r \sim t^{1/3}$ (Fig. 2e, solid line), same as the BMC mechanism. This coarsening behavior is analogous to experimental results in Fig. 1d. At an intermediate ratio $r_0/r_c = 0.5$, the mean droplet size initially does not grow and then increases abruptly, reminiscent of experimental results in Fig. 1e. For even smaller r_0, such as $r_0/r_c = 0.3$, the mean droplet size remains constant over the entire simulation time (Fig. 2c), consistent with experimental results in Fig. 1f. Together, these simulations support that the merging-limited coarsening mechanism with droplet size-dependent merging efficiency underlies the suppressed coarsening of nanoscale coacervates observed in experiments.

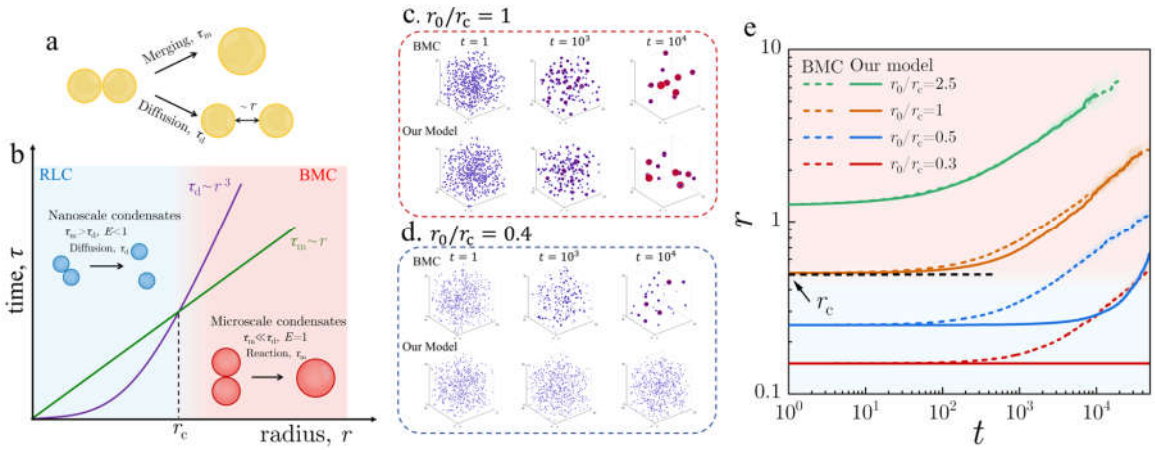

Fig. 2. Scaling analysis and simulations suggest a merging-limited coarsening (MLC) mechanism for nanoscale complex coacervates. (a) Schematic illustrations of the diffusion and merging events that can occur between two nearby droplets at respective timescales τ_d and τ_m. (b) The timescales of diffusion and merging are plotted as a function of droplet radius r. A critical size r_c is derived at $\tau_m = \tau_d$. Above r_c, $\tau_m < \tau_d$ so BMC dominates the growth of droplets with merging efficiency $E = 1$; below r_c, $\tau_m > \tau_d$ so MLC underpins the growth of droplets with $E < 1$. (c) and (d) Snapshots of droplet coarsening at time points ($t = 1, 10^3$ and 10^4) for $r_0/r_c = 1$ and $r_0/r_c = 0.4$, respectively. r_c is the critical size determined by Eq. (1) and is set to unity in all simulations. Each simulation starts with 500 droplets in a $35 \times 35 \times 35$ cubic box. (c) Mean radius of droplets as a function of time for our model (solid lines) and the BMC model (dash lines). Standard deviations (shaded areas) are obtained across 10 simulation replicates with different random seeds.

Theory of diffusion and merging-limited coarsening quantitatively describes experiments.

To comprehensively understand different coarsening mechanisms and quantitatively describe our experimental results, we present a theory that incorporates both diffusion and merging of droplets in their coarsening dynamics [48]:

$$\frac{dr^3}{dt} = \frac{3\phi_0}{8\pi}\frac{k_{\mathrm{diff}}k_{\mathrm{act}}(r)}{k_{\mathrm{diff}} + k_{\mathrm{act}}(r)}, \tag{3}$$

(see supplementary Note 2 for details). Here, $k_{\mathrm{diff}} = 16\pi Dr$ is the rate of encounter for diffusive droplets according to the Smoluchowski theory [49] and k_{act} is the merging rate which accounts for size-dependent merging probability between encountering droplets [50]. Based on Eq. (2), we set $k_{\mathrm{act}}(r) = k_0 e^{-(r_c/r)^2}$ where k_0 is a constant prefactor. ϕ_0 is the volume fraction of droplets in the system, which depends on the initial concentrations of polymers. When merging of droplets occurs at a rate much faster than the diffusion rate, i.e., $k_{\mathrm{act}} \gg k_{\mathrm{diff}}$, Eq. (3) reduces to the classic BMC model [3],

$$\frac{dr^3}{dt} = \frac{k_{\mathrm{B}}T\phi_0}{\pi\eta_0}, \tag{4}$$

which then leads to $r \sim t^{1/3}$. In the other limit, when merging happens at a very low probability so $k_{\mathrm{act}} \ll k_{\mathrm{diff}}$, we obtain the MLC model:

$$\frac{dr^3}{dt} = \frac{3\phi_0}{8\pi}k_{\mathrm{act}}(r). \tag{5}$$

In the limit of $k_{\mathrm{act}} \to 0$, Eq. (5) reduces to $\log r \sim k_{\mathrm{act}}t$, suggesting an exponential increase of r as a function of time (Supplementary Note 2). To demonstrate that, we have replotted experimental coarsening results of PMA/PDDA and PVS/PDDA coacervates in semi-logarithmic coordinates. Results show d_h of nanoscale coacervates formed at relatively low monomer concentration increase linearly over time in semi-logarithmic graphs, confirming an exponential growth via MLC (Supplementary Fig. 9a and Supplementary Fig. 9c). By contrast, linear growth is not observed for microscale coacervates that coarsen via BMC (Supplementary Fig. 9b and Supplementary Fig. 9d). Notably, the MLC we identified here bear some similarities to the merging-limited aggregation of colloidal particles, where the aggregation process also exhibits exponential growth over time [51].

Equation (3) holistically covers both the BMC and MLC regimes. When it is applied to experimental data, the theoretical curves quantitatively capture the coarsening behaviours of coacervates across different concentrations (Fig. 3a). In particular, the proposed theoretical model can capture the abnormal growth of coacervates at intermediate concentrations where a transition between MLC and BMC happens. In addition, the theoretical model predicts that although the

abrupt growth of coacervates following the initial plateau can be faster than the 1/3 power law, the coarsening will eventually approach the BMC limit $r \sim t^{1/3}$ (Supplementary Fig. 10). Such transitions are tentatively observed in experiments which monitor the growth of coacervate over 3 days or more (Supplementary Fig. 11). However, it is noted that, over such extended durations, the accurate measurement of coacervate sizes and monitoring of such a transition may be susceptible to interference from gravity-induced sedimentation of coacervates.

Moreover, it is shown that coacervates initially grow at slow rates in the MLC regime, for which the evolution of coarsening can be described approximately via a hypothesized function of $r \sim t^{\alpha}$ at beginning stages. Our observations align with recent studies that have experimentally showed slow coarsening processes of condensates or coacervates with $\alpha < 1/3$ [22, 52]. Consequently, we seek to ask whether such small α can be captured in our MLC model and how α varies across different condensate sizes. To address the question, we measure α using our experimental data during the initial time period (1-100 min) and plotted them as a function of $d_{\mathrm{h0}}/d_{\mathrm{c}}$ (Supplementary Fig. 12). Experimentally, α increases rapidly as $d_{\mathrm{h0}}/d_{\mathrm{c}}$ approaching 1 and reaches a constant around $1/3$ for $d_{\mathrm{h0}}/d_{\mathrm{c}} > 1$ (Fig. 3b). Such transition is indeed described by a theoretical guideline that present a quick increase in α over $d_{\mathrm{h0}}/d_{\mathrm{c}}$ and a 1/3 plateau regime when $d_{\mathrm{h0}}/d_{\mathrm{c}}$ is larger than 1 (Fig. 3b).

Similar to our observations using complex coacervates, another recent study has showed that condensates formed by the simple coacervation of intrinsically disordered proteins (IDPs), such as hnRNPA2 LCD, resist to grow at various conditions, such as variations of the salt concentrations, urea concentration, and pH [22]. We further apply our theoretical model to analyze the disclosed coarsening data of condensates from the reference [22]. The theoretical BMC curves effectively depict the rapid coarsening dynamics of condensates (Supplementary Fig. 13, red points), while they deviate significantly from describing the coarsening data of condensates at low coarsening rates (Supplementary Fig. 13, black points). Instead, our proposed MLC model well capture these slow coarsening dynamics of condensates (Supplementary Fig. 13). These results demonstrate the universality of MLC in various condensate systems and show the applicability of our theoretical model in describing their anomalously slow coarsening behaviors.

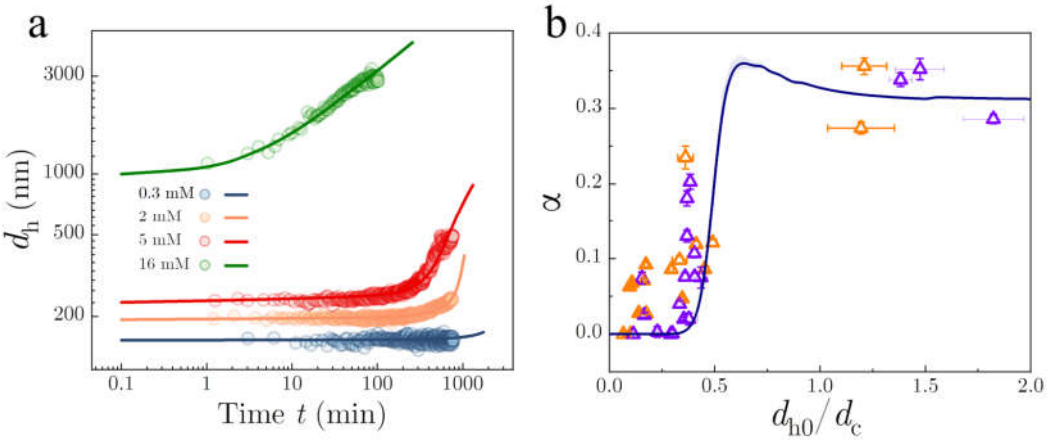

Fig. 3. Theory of diffusion and merging-limited coarsening quantitatively captures the coarsening dynamics of coacervates in experiments. (a) Mean droplet diameter d_h as a function of time from experiments (hollow circles) and theory in Eq. (3) (solid lines). Parameters used in solving Eq. (3) are summarized in Supplementary Table 2. (b) The power-law exponent α of droplet coarsening within an initial period (1-100 min) as a function of d_{h0}/d_c. α are extracted from linearly fitting experimental results on a log-log plot (PMA/PDDA coacervates: purple triangles; PVS/PDDA coacervates: orange triangles). The theoretical α (solid dark blue line) is obtained by fitting theoretical coarsening curves determined using Eq. (3) by a power law relation within the time period of 1-100 min.

MLC underlies the long-term stability of biological condensates.

Having demonstrated the validity of our theory in a few systems, we now apply it to diverse droplet systems. We start by plotting the interfacial tension versus internal viscosity of different types of droplets in a logarithmic plot, in which the contours of the r_c are indicated by straight lines determined by Eq. (1) (Fig. 4a). For typical systems of oil droplets in water, we have $\gamma \approx 20$ mN/m, $\eta \approx 10^{-1}$ Pa · s (viscosity of oil), $\eta_0 \approx 8.9 \times 10^{-4}$ Pa · s (viscosity of water), which leads to extremely small $r_c \approx 1$ nm (Fig. 4a, yellow circles). We can safely assume that oil droplets once nucleated in water should have already passed this threshold size, therefore $r_0/r_c > 1$ and MLC is less relevant for coarsening in oil-water systems. Similarly, all aqueous two-phase systems (ATPS) also have low inverse capillary velocities η/γ. Their r_c values according to Eq. (1) are generally below 10 nm (Fig. 4a, purple circles). By contrast, biological condensates and complex coacervates have much smaller surface tensions ($\gamma \sim 10^{-4} - 10^{-1}$mN/m) and relatively higher viscosities ($\eta \sim 10^{-1} - 10^{3}$ Pa · s). These unique properties of condensates give rise to much larger values of the critical size r_c. For example, based on previously reported parameters, we have estimated r_c for a series of biological condensates and synthetic coacervates, such as

nucleoli, LAF-1, and PGL-3 condensates (Supplementary Table 1). These condensates or coacervates have much larger r_c values, ranging from ~200 nm to a few microns (Fig. 4a, green and red circles). Therefore, we expect MLC to play a pivotal role in the coarsening of biological condensates and complex coacervates, when their sizes are below a few hundred nanometers. In particular, when the droplet size $r \ll r_c$, merging between droplets becomes extremely rare, leading to the long-term stability of nanoscale condensates.

To further verify the crucial role of r_c in determining the coarsening dynamics, we perform experiments on another complex coacervate formed by Poly-L-lysine (PLL) and single stranded RNA. PLL/RNA coacervates are more liquid-like as manifested by their faster merging dynamics compared to coacervates formed by PMA/PDDA and PVS/PDDA (Supplementary Fig. 14). The r_c of the PLL/RNA coacervate is estimated to be 165 nm that is about two- to three- fold smaller than those of PMA/PDDA and PVS/PDDA coacervates (Supplementary Fig. 8). Consistent with our theoretical expectations, we find that starting with similar initial sizes ~200 nm, PLL/RNA coacervates grow quickly following a power-law function with an exponent close to 1/3 as predicted by the BMC theory, in striking contrast to the slow and suppressed growth of PMA/PDDA and PVS/PDDA coacervates (Fig. 4b). These results suggest that the coarsening dynamics is highly sensitive to the ratio between droplet size r and the critical size r_c, which in turn is determined by the physical properties of the condensates. The developed theoretical framework, Eqs. (1) and (3), in this work thus enables quantitative predictions on the coarsening dynamics of diverse droplet systems.

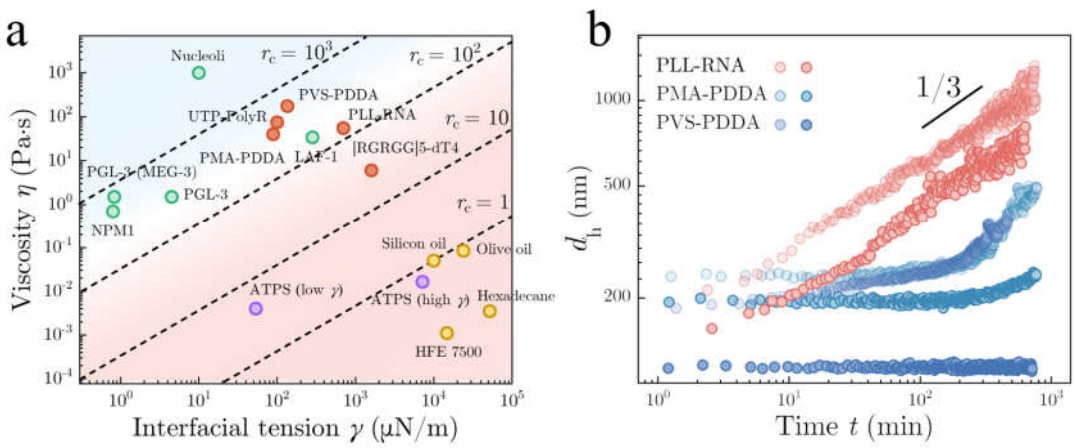

Fig. 4. MLC underpins the slow coarsening and long-term stability of biological condensates. (a) A diagram summarizes the viscosity and interfacial tensions of droplets across

different systems: biological condensates (green circles), complex coacervates (red circles), aqueous two-phase systems (ATPS, purple circles), and oil-water (yellow circles). Biological condensates and complex coacervates typically locate in the top left regime of the diagram with high viscosity-to-interfacial tension ratios and thus large critical sizes r_c. MLC can dominate the coarsening dynamics of droplets below a few hundred nanometers, leading to suppressed coarsening and long-term stability of biological condensates. (b) d_h plotted as a function of time for three different complex coacervates. PMA/PDDA and PVS/PDDA systems have relatively large r_c and thus coarsen via the MLC mechanism, while the PLL/RNA system has a smaller r_c which coarsens quickly according to the BMC theory.

Discussions

In this work, we introduce a general merging-limited coarsening (MLC) mechanism that manifests extremely slow coarsening rate and leads to the long-term size stability of nanoscale condensates. By applying the scaling analysis, we find that small condensates in the MLC regime do not have enough time to merge upon diffusive encounter, leading to multiple contacts before merging, in contrast to the classic BMC mechanism wherein condensates readily merge upon contact. This unique characteristic leads to a drastically slow coarsening in MLC, as shown in experiments and Monte Carlo simulations. We further derive an analytical model that accounts for a size-dependent merging efficiency of droplets. The resultant model quantitatively describes the experimental results across different conditions and coarsening mechanisms, i.e., BMC and MLC. Our merging-limited coarsening model presents a generic framework that could be extended to incorporate other previously reported strategies for stabilizing condensates, such as interfacial clusters [12, 53] and surface charge [54-56]. These strategies under the scheme of merging-limited coarsening may reduce the merging efficiency of condensates further and thus lead to more suppressed coarsening. Interestingly, in addition to reduced merging of droplets, recent works also suggest the diffusion of molecules across the interface of condensates can also be reduced [57, 58], leading to an inhibited coarsening that is much slower than predictions by the Lifshitz-Slyozov-Wagner theory of Ostwald ripening [57]. Our work combined with literature emphasizes the rugged energy landscape and the corresponding suppressed coarsening of condensates at small scales.

Our results also suggest that stable nanoscale condensates often appear at relatively low macromolecular concentrations. Consistently, recent experiments and molecular dynamic simulations have shown that condensates formed at low and intermediate concentrations exhibit slow coarsening phenomena [20, 21, 23, 42, 59, 60]. The low concentration regime is much

relevant to biological systems, as the physiological concentrations of phase-separated biomacromolecules range from nanomolar to micromolar, close to the phase separation threshold concentrations [20]. Moreover, we present in a diagram that many biological condensates or coacervates exhibit intrinsically large critical sizes due to their relatively high viscosity and low interfacial tension. Having large critical sizes means that nanoscale condensates are likely to grow through the MLC mechanism with very low coarsening rates. Therefore, our work may have provided the mechanistic insights for understanding the long-term stability of condensates widely observed in living cells and *in vitro* systems.

Methods

Preparation of complex coacervates: Stock solutions of poly(methacrylic acid, sodium salt) (PMA, Sigma-Aldrich, 674044), poly(vinylsulfonic acid, sodium salt) (PVS, Macklin, P909334), Poly(diallyldimethylammonium chloride) (PDDA, Sigma-Aldrich, 522376), Poly-L-lysine (PLL, Sigma-Aldrich, p2636), and RNA (IDT, UGAGAAUGAAUAGAAUGAAUAA) were firstly prepared at high concentrations using Milli-Q water (18.2 MΩ, pH=7). The stock solutions were diluted according to designed c_{m}. Complex coacervates were formed by gently mixing diluted oppositely charged polymer solutions at a charge-balanced neutral stoichiometry.

Dynamic light scattering (DLS): DLS measurements were preformed using a Zetasizer Pro (Malvern Instruments, UK) with a measurement range from 0.3 nm to 10 μm. Complex coacervate samples with volume of approximately 1mL were transferred into transparent cuvettes (DTS0012, Malvern) using a pipette. The cuvettes were subsequently sealed with a plastic cap and placed into the Zetasizer Pro machine. A He-Ne laser (633 nm) was used to illuminate the sample and the intensity of light scattered at a constant angle of 173° was measured using a photodiode. The program presets the viscosity of water (1.0 mPa) and the refractive index (1.38) for the measurement, settled at room temperature (25 ℃) with a 120 s equilibration time. To determine the hydrodynamic diameters d_{h0}, three measurements were carried out for each sample, and at least three independent samples were measured to obtain a mean ± SD. To conduct the long-term monitoring of d_h, the program was set to continuously record the hydrodynamic diameters at intervals ranging from 1 to 3 minutes.

Optical microscopy: The bright-filed images were captured by an inverted fluorescence microscope (Olympus) equipped with a differential interference contrast (DIC) filter. The sample was loaded into customized chambers fabricated using spacers (ThermoFisher, S24737) sandwiched by two coverslides at a 120 μm gap. The coverslides were cleaned by ethanol and water to remove contaminants and coated with mPEG-Silane (Aladdin, S164281) to reduce the adhesion of coacervates onto surfaces. The coated slides were carefully rinsed using Milli-Q water to remove chemical residues, followed by drying inside 65 ℃ oven for 1 hour.

Transmission electron microscopy (TEM): Carbon-coated copper grids were firstly discharged by a Glow Discharge Cleaning System to become hydrophilic (Pelco EasiGlow 91000). 5 μL samples containing complex coacervates was loaded onto the grids (Ted Pella, Inc.). The samples on grids were negatively stained with uranyl acetate (UA), followed by general removal of excess staining solutions using a filter paper wick, and subsequent air-drying before imaging. The TEM were performed using a FEI Tecnai G2 20 facility at the Electron Microscope Unit (EMU) at the University of Hong Kong.

Simulations: Simulations were performed in MATLAB. Initially, a total of N droplets were generated in a three-dimensional box of dimensions $35 \times 35 \times 35$ using random seeds, with periodic boundary conditions. At each time step, droplets were allowed to move randomly in three dimensions at a distance set by the mean square displacement (MSD), that is $\langle x \rangle^2 = 6D\Delta t$ where the diffusion coefficient was determined by the Stoke-Einstein equations $D = k_B T/(6\pi\eta r)$. In the case of BMC, if droplets overlapped, they were merged to form a single large droplet located at their center of mass. The size of new droplet was determined by the volume and mass conservation of two overlapped droplets. In our modified model, in the case of overlapping droplets, the merging efficiency E was calculated by Eq. (2) using the mean radius of two overlapped droplets. A random number was generated as P for each merging counter. If $P \leq E$, the two droplets were merged as previously described. On the other hand, if $P > E$, the droplets would move away from each other in opposite directions parallel to the line connecting their centers. The mean radius r of all droplets was calculated and recorded at each timepoint.

Coacervate fusion experiments: Coacervate samples were transferred into a customized chamber and observed under an optical microscope. Time-lapse movies were recorded using a 40x objective.

The aspect ratio (AR) was determined by fitting an ellipse to the shape of two coacervate droplets and calculating the AR=L/S, where L and S are the long and short axes of the ellipse using a reported MATLAB script [61]. The change of AR over time is fitted using a function defined as $AR = AR_f + (AR_0 - AR_f)e^{-t/\tau}$, where t is time, τ is the relaxation time, AR_0 and AR_f are initial and final aspect ratios respectively. The characteristic length l was defined as the geometrical mean where $l = \sqrt{r_1 r_2}$, where r_1 and r_2 are the initial radius of two contacting droplets. Plot of τ vs. l were fit linearly for different coacervates to determine the inverse capillary velocity η/σ.

Rheology: The measurement of viscosity was performed using a stress-controlled Anton Paar MCR301 rheometer with Peltier temperature control. A cone plate with a radius of 25 mm and a cone angle of 1° was used as the top geometry. Complex coacervates were formed at 50 mM in bulk phase and centrifuged at 4000g for 10 minutes. The dilute phase was removed from the top and the bottom coacervate phase was extracted. Coacervate samples were firstly loaded onto the bottom surface of the rheometer, and the top plate was then lowered onto samples with a fixed gap of 0.051 mm. The shear rate is applied ranging from 0.001 to 1000 1/s for the viscosity measurement.

Conflict of interest

The authors declare that they have no competing interests.

Acknowledgements

We thank Dr. Wei Guo and Dr. Xiufeng Li for useful discussions. This work was supported by the General Research Fund (Nos. 17306221, 17317322, and 17306820) from the Research Grants Council (RGC) of Hong Kong, as well as the National Natural Science Foundation of China (NSFC)-RGC Joint Research Scheme (N_HKU718/19). H.C.S. was funded in part by the Croucher Senior Research Fellowship from Croucher Foundation and the Health@InnoHK program of the Innovation and Technology Commission of the Hong Kong SAR Government. Y. Z. was supported by a startup fund at Johns Hopkins University.

Author contributions

F.C. and Y.Z. conceptualized and designed the project. F.C. performed the experiments, simulations, data analysis. F.C. and Y.Z. built the analytical models. Y.Z. and H.C.S. supervised the project. F.C. wrote the manuscript, and Y.Z. and H.C.S revised it.

References

1. Lee, D.S., N.S. Wingreen, and C.P. Brangwynne, *Chromatin mechanics dictates subdiffusion and coarsening dynamics of embedded condensates.* Nature Physics, 2021. **17**(4): p. 531-538.
2. Berry, J., et al., *RNA transcription modulates phase transition-driven nuclear body assembly.* Proceedings of the National Academy of Sciences, 2015. **112**(38): p. E5237-E5245.
3. Berry, J., C.P. Brangwynne, and M. Haataja, *Physical principles of intracellular organization via active and passive phase transitions.* Reports on Progress in Physics, 2018. **81**(4): p. 046601.
4. Zhang, Y., et al., *Mechanical frustration of phase separation in the cell nucleus by chromatin.* Physical review letters, 2021. **126**(25): p. 258102.
5. Ratke, L. and P.W. Voorhees, *Growth and coarsening: Ostwald ripening in material processing*. 2002: Springer Science & Business Media.
6. Rosowski, K.A., et al., *Elastic ripening and inhibition of liquid–liquid phase separation.* Nature physics, 2020. **16**(4): p. 422-425.
7. Lyon, A.S., W.B. Peeples, and M.K. Rosen, *A framework for understanding the functions of biomolecular condensates across scales.* Nature Reviews Molecular Cell Biology, 2021. **22**(3): p. 215-235.
8. Shin, Y. and C.P. Brangwynne, *Liquid phase condensation in cell physiology and disease.* Science, 2017. **357**(6357).
9. Brangwynne, C.P., et al., *Germline P granules are liquid droplets that localize by controlled dissolution/condensation.* Science, 2009. **324**(5935): p. 1729-1732.
10. Alberti, S., A. Gladfelter, and T. Mittag, *Considerations and challenges in studying liquid-liquid phase separation and biomolecular condensates.* Cell, 2019. **176**(3): p. 419-434.
11. Elbaum-Garfinkle, S., et al., *The disordered P granule protein LAF-1 drives phase separation into droplets with tunable viscosity and dynamics.* Proceedings of the National Academy of Sciences, 2015. **112**(23): p. 7189-7194.
12. Folkmann, A.W., et al., *Regulation of biomolecular condensates by interfacial protein clusters.* Science, 2021. **373**(6560): p. 1218-1224.
13. Feric, M. and C.P. Brangwynne, *A nuclear F-actin scaffold stabilizes ribonucleoprotein droplets against gravity in large cells.* Nature cell biology, 2013. **15**(10): p. 1253-1259.
14. Yan, V.T., et al., *A condensate dynamic instability orchestrates actomyosin cortex activation.* Nature, 2022. **609**(7927): p. 597-604.
15. Loose, M., et al., *Spatial regulators for bacterial cell division self-organize into surface waves in vitro.* Science, 2008. **320**(5877): p. 789-792.
16. Nakashima, K.K., et al., *Active coacervate droplets are protocells that grow and resist Ostwald ripening.* Nature Communications, 2021. **12**(1): p. 1-11.

17. Zwicker, D., et al., *Growth and division of active droplets provides a model for protocells.* Nature Physics, 2017. **13**(4): p. 408-413.
18. Zwicker, D., A.A. Hyman, and F. Jülicher, *Suppression of Ostwald ripening in active emulsions.* Physical Review E, 2015. **92**(1): p. 012317.
19. Wang, Z., et al., *Cellular proteins act as surfactants to control the interfacial behavior and function of biological condensates.* Developmental cell, 2023.
20. Ray, S., et al., *Mass photometric detection and quantification of nanoscale α-synuclein phase separation.* Nature Chemistry, 2023.
21. Morin, J.A., et al., *Sequence-dependent surface condensation of a pioneer transcription factor on DNA.* Nature Physics, 2022. **18**(3): p. 271-276.
22. Van Lindt, J., et al., *A generic approach to study the kinetics of liquid–liquid phase separation under near-native conditions.* Communications biology, 2021. **4**(1): p. 1-8.
23. Peng, S., et al., *Phase separation at the nanoscale quantified by dcFCCS.* Proceedings of the National Academy of Sciences, 2020. **117**(44): p. 27124-27131.
24. Lan, C., et al., *Quantitative real-time in-cell imaging reveals heterogeneous clusters of proteins prior to condensation.* Nature Communications, 2023. **14**(1): p. 4831.
25. Kar, M., et al., *Phase-separating RNA-binding proteins form heterogeneous distributions of clusters in subsaturated solutions.* Proceedings of the National Academy of Sciences, 2022. **119**(28): p. e2202222119.
26. Chong, S., et al., *Imaging dynamic and selective low-complexity domain interactions that control gene transcription.* Science, 2018. **361**(6400): p. eaar2555.
27. Spannl, S., et al., *Biomolecular condensates in neurodegeneration and cancer.* Traffic, 2019. **20**(12): p. 890-911.
28. Zeng, M., et al., *Phase Transition in Postsynaptic Densities Underlies Formation of Synaptic Complexes and Synaptic Plasticity.* Cell, 2016. **166**(5): p. 1163-1175.e12.
29. Sabari, B.R., et al., *Coactivator condensation at super-enhancers links phase separation and gene control.* Science, 2018. **361**(6400).
30. Cho, W.-K., et al., *Mediator and RNA polymerase II clusters associate in transcription-dependent condensates.* Science, 2018. **361**(6400): p. 412-415.
31. Larson, A.G., et al., *Liquid droplet formation by HP1α suggests a role for phase separation in heterochromatin.* Nature, 2017. **547**(7662): p. 236-240.
32. Strom, A.R., et al., *Phase separation drives heterochromatin domain formation.* Nature, 2017. **547**(7662): p. 241-245.
33. Nott, T.J., et al., *Phase transition of a disordered nuage protein generates environmentally responsive membraneless organelles.* Molecular cell, 2015. **57**(5): p. 936-947.
34. Abbas, M., et al., *Peptide-based coacervates as biomimetic protocells.* Chemical Society Reviews, 2021.
35. Rumyantsev, A.M., N.E. Jackson, and J.J. de Pablo, *Polyelectrolyte Complex Coacervates: Recent Developments and New Frontiers.* Annual Review of Condensed Matter Physics, 2020. **12**.
36. Cook, A.B., S. Novosedlik, and J.C. van Hest, *Complex Coacervate Materials as Artificial Cells.* Accounts of Materials Research, 2023. **4**(3): p. 287-298.
37. Guo, W., et al., *Tuning Material States and Functionalities of G-Quadruplex-Modulated RNA-Peptide Condensates.* Journal of the American Chemical Society, 2023. **145**(4): p. 2375-2385.

38. Lu, T. and E. Spruijt, *Multiphase complex coacervate droplets.* Journal of the American Chemical Society, 2020. **142**(6): p. 2905-2914.
39. Abbas, M., et al., *A short peptide synthon for liquid–liquid phase separation.* Nature Chemistry, 2021: p. 1-9.
40. Lipiński, W.P., et al., *Biomolecular condensates can both accelerate and suppress aggregation of α-synuclein.* Science Advances, 2022. **8**(48): p. eabq6495.
41. Sun, Y., et al., *Phase-separating peptides for direct cytosolic delivery and redox-activated release of macromolecular therapeutics.* Nature Chemistry, 2022. **14**(3): p. 274-283.
42. Zhang, Y., et al., *Decoding the physical principles of two-component biomolecular phase separation.* Elife, 2021. **10**: p. e62403.
43. He, G., et al., *Phase-separating pyrenoid proteins form complexes in the dilute phase.* Communications Biology, 2023. **6**(1): p. 19.
44. Martin, E.W., et al., *A multi-step nucleation process determines the kinetics of prion-like domain phase separation.* Nature communications, 2021. **12**(1): p. 1-12.
45. Shimobayashi, S.F., et al., *Nucleation landscape of biomolecular condensates.* Nature, 2021. **599**(7885): p. 503-506.
46. Brangwynne, C.P., T.J. Mitchison, and A.A. Hyman, *Active liquid-like behavior of nucleoli determines their size and shape in Xenopus laevis oocytes.* Proceedings of the National Academy of Sciences, 2011. **108**(11): p. 4334-4339.
47. Siggia, E.D., *Late stages of spinodal decomposition in binary mixtures.* Physical review A, 1979. **20**(2): p. 595.
48. Rice, S.A., *Diffusion-limited reactions*. 1985: Elsevier.
49. Smoluchowski, M.v., *Versuch einer mathematischen Theorie der Koagulationskinetik kolloider Lösungen.* Zeitschrift für physikalische Chemie, 1918. **92**(1): p. 129-168.
50. Collins, F.C. and G.E. Kimball, *Diffusion-controlled reaction rates.* Journal of colloid science, 1949. **4**(4): p. 425-437.
51. Lin, M., et al., *Universality in colloid aggregation.* Nature, 1989. **339**(6223): p. 360-362.
52. Liu, X., et al., *Early stage kinetics of polyelectrolyte complex coacervation monitored through stopped-flow light scattering.* Soft Matter, 2016. **12**(44): p. 9030-9038.
53. Cuylen, S., et al., *Ki-67 acts as a biological surfactant to disperse mitotic chromosomes.* Nature, 2016. **535**(7611): p. 308-312.
54. Welsh, T.J., et al., *Surface electrostatics govern the emulsion stability of biomolecular condensates.* Nano letters, 2022.
55. Cochard, A., et al., *RNA at the surface of phase-separated condensates impacts their size and number.* Biophysical Journal, 2022.
56. Toyama, Y., et al., *Surface electrostatics dictate RNA-binding protein CAPRIN1 condensate concentration and hydrodynamic properties.* Journal of Biological Chemistry, 2023. **299**(1).
57. Lee, C.F., *Scaling law and universal drop size distribution of coarsening in conversion-limited phase separation.* Physical Review Research, 2021. **3**(4): p. 043081.
58. Zhang, Y., et al., *Interface resistance of biomolecular condensates.* bioRxiv, 2023: p. 2022.03.16.484641.
59. Ranganathan, S. and E.I. Shakhnovich, *Dynamic metastable long-living droplets formed by sticker-spacer proteins.* Elife, 2020. **9**: p. e56159.

60. Xu, B., et al., *Rigidity enhances a magic-number effect in polymer phase separation.* Nature Communications, 2020. **11**(1): p. 1561.
61. Rhine, K., et al., *Poly (ADP-ribose) drives condensation of FUS via a transient interaction.* Molecular cell, 2022. **82**(5): p. 969-985. e11.